Dr JAN A. SZANTYR
Institute of Fluid Flow Machinery
Polish Academy of Sciences
Gdańsk

A NUMERICAL METHOD FOR ANALYSIS OF CAVITATION ON MARINE PROPELLERS

SUMMARY

The paper presents a new version of the unsteady deformable lifting surface method for analysis of propeller operation in the nonuniform velocity field behind the ship hull. This new version is concentrated on possibly accurate modelling of three different forms of cavitation typical of marine propellers, namely sheet, bubble, and tip vortex cavitation. The paper presents theoretical background of the method and selected examples of the initial experimental verification.

Introduction

Analysis of different hydrodynamic aspects of marine propeller operation in the non-uniform flow behind ship stern has already become a standard element of the propeller design process. Application of theoretical methods for this purpose instead of cavitation tunnel experiments is advantageous in terms of time and cost. The method presented in this paper results from a compromise between possibly realistic theoretical model of the physical phenomena and limited computational resources available for an average propeller designer. The method is based on the unsteady lifting surface theory modified especially to integrate the time-dependent cavitation phenomena into the lifting surface model. This approach is named the deformable lifting surface theory, as the cavities change the initial geometry of the lifting surface. For each analysed blade position in the non-uniform inflow the kinematic boundary condition on the blade and dynamic boundary condition on the cavity surface are evaluated and the resulting distribution of cavity expansion (or contraction) is calculated. This leads to evaluation of the cavity geometry for every analysed blade position. The cavity geometry established in the previous blade position is regarded as a deformation of the lifting surface in the current blade position, affecting the kinematic and dynamic boundary conditions. In this way cavitation is modelled as a continuous process in which the previous development of the cavity affects its current situation. The unsteadiness of the flow itself is accounted for by introducing the free vortex surfaces of variable, time-dependent intensity into the propeller slipstream. The variation of vorticity on these sheets follows the changes of the hydrodynamic loading on the propeller blades and through participation in calculation of the induced velocity it provides the feedback between the history of the flow and the current kinematic situation at the propeller.

Computational model of the propeller

The lifting surface theory employed in this analysis is based on modelling the hydrodynamic loading on the propeller blades with distribution of vorticity and on modelling the blade thickness with distribution of sources and sinks. Both these types of singularities are located on the surfaces built of the mean lines of propeller blade sections. Following the classical linearised approach the effects of hydrodynamic loading and thickness are separated from each other. It is further assumed that the unsteadiness of flow is reflected only in the hydrodynamic loading, while the intensity of sources and sinks corresponds to circumferentially average inflow. The kinematic boundary condition is the basis for the formulation of the lifting surface equation. This condition requires the resultant relative velocity of flow at the lifting surface to be tangent to this surface.

$$\frac{1}{4\pi}\left[\int_{S_p}\int \bar{n}\bar{\gamma}_p \nabla\left(-\frac{1}{r_p}\right)dS+\int_{S_f}\int \bar{n}\bar{\gamma}_f \nabla\left(-\frac{1}{r_f}\right)dS+\int_{S_p}\int (q_p+q_{pc})\frac{\partial}{\partial n}\left(-\frac{1}{r_p}\right)dS\right]+$$

$$+(\bar{V}+\bar{\omega}R)\bar{n}=0 \qquad (1)$$

where:

$\bar{n}$ – unit length vector normal to the lifting surface

$\bar{\gamma}_p$ – vorticity distribution on the lifting surfaces
$\bar{\gamma}_f$ – vorticity distribution in the free vortex surfaces
q_p – source distribution modelling blade thickness
q_{pc} – source distribution modelling quasi-steady sheet cavity
r_p – distance between area element and the point of calculation
s_p – area of the lifting surfaces
S_f – area of the free vortex surfaces
$\bar{V}$ – inflow velocity
$\bar{\omega}$ – angular velocity of propeller rotation
R – radius at which the point of calculation is located

In the numerical evaluation of equation (1) the continuous distribution of vorticity and sources over the lifting

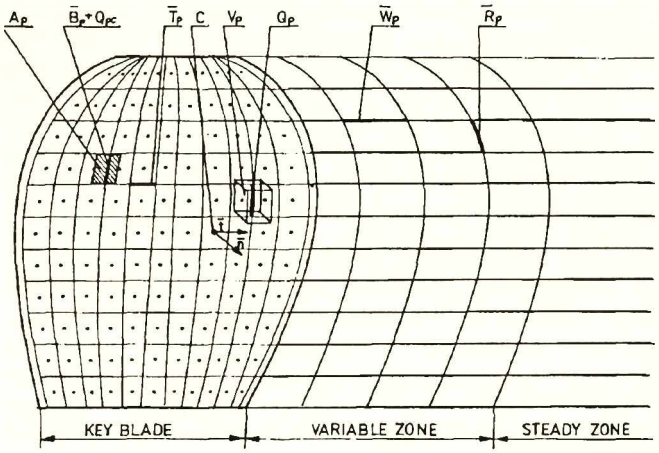

Fig. 1. Discrete Vortex/Source Model of the Propeller Blade

surfaces is replaced by a discrete distribution of vortex and source elements, shown schematically in Fig. 1. Fifteen bound vortex elements Bp are distributed along each of the eleven chordwise strips. Each element represents vorticity concentrated from an area element A_p. In order to fulfil the theorem about conservation of vorticity the trailing vortex elements T_p are introduced. After leaving the blade trailing edge the trailing vortices form the free vortex surfaces. One of the blades is distinguished as the key blade and on this blade control points C are located in the middle of quadrangles built of the adjacent elements B_p and T_p. Control points are used for evaluation of the kinematic boundary condition. Consequently, equation (1) is converted into a system of linear equations, each of which corresponds to one control point. In order to close the system, the Kutta condition is used bringing the number of unknown Bp intensities to the number of control points. Intensities of the sources Q_p, modelling the blade thickness, are calculated on the assumption that each of them should cancel inflow to the blade volume element Vp. The section of the free vortex surface immediately behind the key blade is distinguished as the variable zone. The vorticity distribution in this zone reflects the history of varying hydrodynamic loading on the key blade as the blade moves through the non-uniform inflow velocity field. The vorticity distribution in this zone is continuously updated during the analysis. The remaining part of the free vortex system forms the steady zone in which the vorticity distribution corresponds to the cicumferentially averaged inflow velocity field. The system of linear equations is solved for every analysed blade position in the non-uniform inflow velocity field, leading to the vorticity distribution. Then the resultant flow velocity may be calculated using the Biot-Savart formula and the pressure distribution on the blade may be evaluated following the Bernoulli equation for unsteady flows.

Detection and modelling of cavitation

Three different forms of cavitation, shown schematically in Fig. 2, may be detected and modelled on the propeller blade:
- sheet cavitation
- tip vortex cavitation
- bubble cavitation.

Detection of the sheet cavitation inception is based on the analysis of behaviour of the cavitation nuclei in the region of 5% of the blade section chord length from the leading edge. The basic tool for this analysis is the Rayleigh-Plesset equation for the dynamics of an isolated, spherical, vapour-filled bubble [2]:

$$\frac{d^2 R_b}{dt^2} = \left[\frac{\Delta p}{\rho} - \frac{3}{2}\left(\frac{dR_b^2}{dt}\right) - \frac{2S}{\rho R_b} - \frac{4\mu}{\rho R_b}\frac{dR_b}{dt}\right]\frac{1}{R_b} \qquad (2)$$

where:
R_b – bubble radius
Δp – pressure difference responsible for bubble growth/collapse
S – surface tension of water
μ – dynamic viscosity coefficient of water
ρ – density of water.

The analysis is performed for all chordwise sections, both for the suction and presure side of the blade. Equation (2) is solved in a stepwise manner using the Runge-Kutta method. Initial conditions are $R_b = R_o$ and $dR_b/dt = 0$, where R_o is the characteristic radius of the cavitation nuclei normally present in water. The inception of cavitation is assumed when R_b reaches prescribed critical value Rc, which in present analysis is taken equal 0.25 mm. If this happens within 5% of the chord length from the leading edge, inception of sheet cavitation is signalled. If Rb exceeds Rc outside the 5% region, the inception of bubble cavitation is defined. The region of bubble cavitation

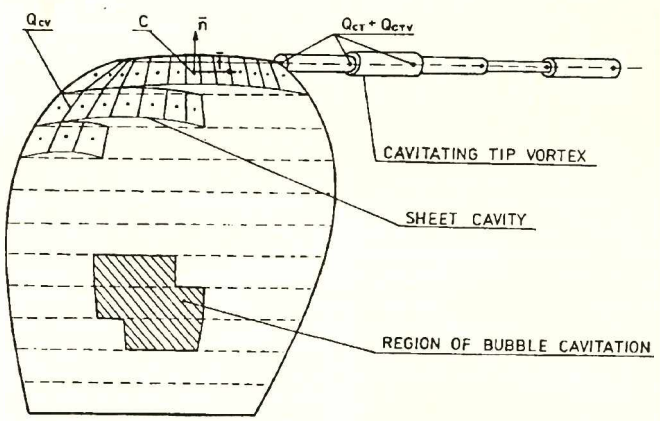

Fig. 2. Model of the Caviation Phenomena on the Propeller Blade

extends in the chordwise direction until the local value of R_b obtained from (2) again falls below R_c (cf. Fig. 2). The chordwise extent of sheet cavity corresponds to the area where the static pressure is lower than the critical vapour pressure at given temperature. It is assumed that the dynamics of the sheet cavity may be modelled by an additional system of sources Q_{cv} coinciding with Q_p. The intensity of Q_{cv} may be obtained from the dynamic bounary condition on the sheet cavity surface. This condition stipulates equilibrium of forces on the cavity boundary and it has the following form:

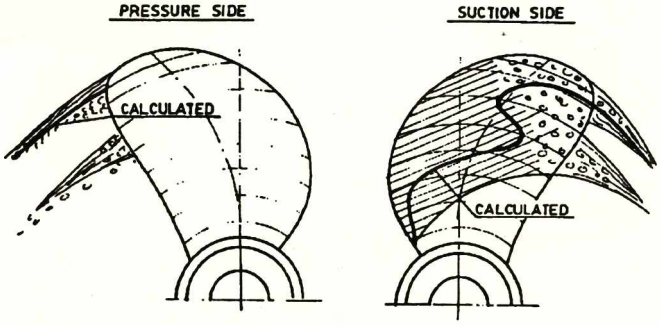

Fig. 3. Calculated and Observed Cavitation Pattern on the Propeller Model PI at J = 0.393 and σ = 2.46

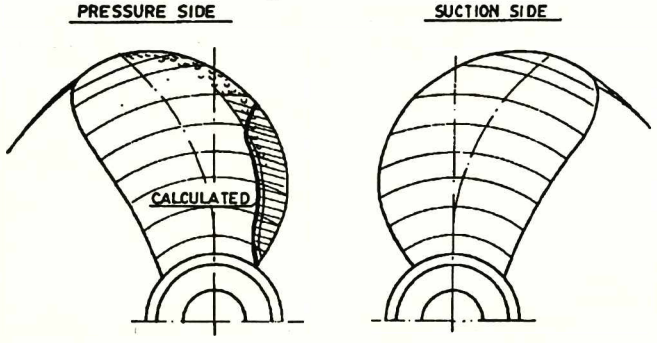

Fig. 4. Calculated and Observed Cavitation Pattern on the Propeller Model PI at J = 0.99 and σ = 1.266

$$\frac{1}{2\pi V_\infty^2}\int_{S_c}\int \frac{dq_{cv}}{dt}\frac{\partial}{\partial n}\left(-\frac{1}{r_p}\right) = -C_p - \sigma - \frac{4S}{\rho V_\infty^2 R_c} \tag{3}$$

where:

R_c – radius of curvature of the cavity cross-section

S_o – area covered by the sheet cavity

q_{cv} – continuous distribution of sources corresponding to Q_{cv}

C_p – local pressure coefficient

σ – local cavitation number.

Equation (3) may be applied to every control point within the sheet cavity area, thus forming the system of equations for Q_{cv}. After this system is solved, the distribution of normal deformation velocity of the cavity boundary is calculated. Assuming this velocity remains constant in the time step separating the analysed blade positions, the sheet cavity thickness distribution at the end of this time step may be calculated. This quasi-steady thickness distribution of the sheet cavity is modelled by a system of discrete sources Qpc in the manner similar to the blade thickness. The procedure for detection of the cavitating tip vortex is based on the combined Rankine vortex model [3]. This model assumes that the vorticity is uniformly concentrated inside a vortex core having radius R_l. Outside this core the flow is irrotational, while the core itself rotates as a rigid body. Consequently, the minimum pressure occurs in the core centre and it is equal to:

$$C_{p\min} = -\frac{1}{2\pi^2 V_\infty^2}\left(\frac{\Gamma}{R_l}\right)^2 \tag{4}$$

where:

Γ – circulation of the tip vortex

V_∞ – resultant undisturbed flow velocity.

In a practical solution it is assumed that R_l is equal to the boundary layer thickness at the trailing edge, evaluated using the method of Truckenbrodt. The value of Γ is supplied by the lifting surface algorithm. In order to initiate the tip vortex cavitation the pressure C_{pmin} must fall low enough to burst cavitation nuclei of a prescribed size. The behaviour of nuclei inside the vortex core is again analysed using the equation (2). The inception of tip vortex cavitation is indicated when R_b reaches the prescribed value R_c. Due to variable intensity of the tip vortex the calculated diameter of the cavitating kernel may also vary (cf. Fig. 2). The quasi-steady displacement effect of the cavitating vortex kernel is modelled by a system of sources Q_{ct}, while the dynamic effect is simulated by the sources Q_{ctv}.

Comparison of the numerical and experimental results

The initial experimental verification of the new method is based on the results of cavitation tunnel experiments with two propeller models, P1 and P2. In order to verify different aspects of the theory the model P1 was tested in the uniform velocity field while the model P2 was tested in the simulated three-dimensional non-uniform inflow velocity field. Fig. 3 presents a comparison of calculated and experimentally observed cavitation phenomena on the model P1 at a relatively low advance coefficient J, with cavitation present on the suction side. Fig. 4 shows a similar comparison at a much higher advance coefficient J and lower cavitation number σ, when cavitation develops on the pressure side of the blade. Fig. 5 presents a comparison of calculated and experimental cavitation inception diagram

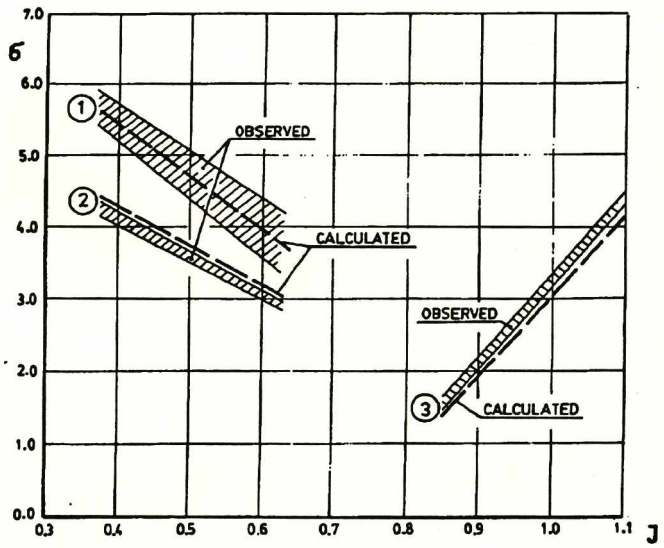

Fig. 5. Cavitation Inception Diagram of the Propeller Model PI

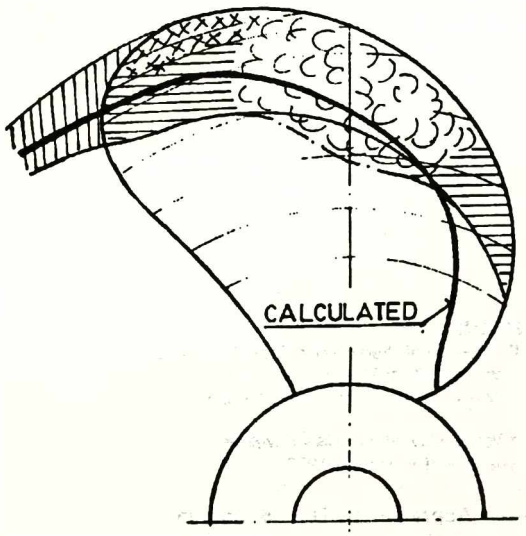

Fig. 6. Calculated and observed cavitation pattern on the propeller model P2 at Θ = 0° σ = 1.92 K_T = 0.275

of the model P1. In this diagram line 1 denotes inception of the cavitating tip vortex, line 2 - inception of sheet cavitation on suction side and line 3 - inception of sheet cavitation on pressure side. Finally, Fig. 6 shows a comparison of calculated and observed cavitation phenomena on the model P2 at the top blade position in the non-uniform inflow. The above presented comparison demonstrates the typical accuracy of the theoretical procedure in prediction of the physically complicated phenomena of cavitation on marine propellers. This accuracy is fully comparable with that of the cavitation tunnel experiments, but at a considerably lower expense of time and money.

REFERENCES

1. Cummings D.E.: Numerical Prediction of Propeller Characteristics. Journal of Ship Research, vol. 17, 1973 No. 1.
2. Knapp R.T., Daily J.W., Hammitt F.G.: Cavitation. Mc. Graw-Hill, New York 1970.
3. Latorre R.: Tip Vortex Cavitation Noise Envelope. Proc. of 17th Symp. on Naval Hydrodynamics, The Hague 1988.

Appraised by Doc. dr hab. inż. T. Koronowicz